Eur. Phys. J. B (2026)99:99
https://doi.org/10.1140/epjb/s10051-026-01202-6

THE EUROPEAN PHYSICAL JOURNAL B

Research - Condensed Matter

Exploring the structural and electronic properties of piperazinium bis (trifluoroacetic acid): DFT insights into optimization, spectral, NBO, NLO, Hirshfeld surface, and Fukui analysis

V. Vijayalakshmi[1], K. Sivakumar[2], V. Ragavendran[3], J. Janczak[4], and N. Kanagathara[1,a]

[1] Department of Physics, Saveetha School of Engineering, Saveetha Institute of Medical and Technical Sciences, Saveetha University, Thandalam, Chennai 602 105, India
[2] Department of Chemistry, School of Sciences, Vels Institute of Science Technology & Advanced Studies (VISTAS), Pallavaram, Chennai 600117, India
[3] Department of Physics, Rajalakshmi Engineering College, Thandalam, Chennai 602 105, India
[4] Institute of Low Temperature and Structure Research, Polish Academy of Sciences, Okolna 2 Str., 50-422 Wroclaw, Poland

Received 2 February 2026 / Accepted 4 June 2026

Abstract. Organic single crystals of piperazinium bis (trifluoroacetic acid) (PTFA) was synthesized by the slow evaporation method. The centrosymmetric nature of the PTFA crystal was confirmed through single crystal XRD analysis with the P-1 space group. The molecular structure of PTFA was optimized by Density functional theory (DFT) with the B3LYP 6–311 + + G (d, p) basis set to calculated the structural parameters of the compound were compared with the experimental XRD data. The presence of various functional groups and their frequencies were confirmed through FT-IR spectral analysis, based on the potential energy distribution (PED) used for assignments and correlations of the compound's fundamental modes. The electronic transition spectrum of the PTFA molecule was obtained via UV–Vis spectroscopy in various solvents. The analysis of HOMO & LUMO molecular orbitals indicates a significant charge transfer, while Natural Bond Orbital (NBO) analysis revealed donor–acceptor interactions. The molecular electrostatic potential (MEP) and Fukui functions, derived from Mulliken charges, identified a reactive region of the molecule. The chemical bonding was explored through Electron Localization Function (ELF) & Localized Orbital Locator (LOL) analyses and the weak interactions was identified in RDG analysis with inter & intra-fragment interactions illustrated by scatter plots. The first-order hyperpolarization calculation confirms the nonlinear optical activity of the PTFA crystal. Besides, the Hirshfeld surface analysis and 2D fingerprint maps were used for quantitative mapping of intermolecular interactions.

1 Introduction

Piperazine ($C_4H_{10}N_2$) is a well-known organic compound consisting of a six-membered ring with two nitrogen atoms positioned diagonally opposite each other [1–3]. Piperazine is a secondary amine were originally named due to their chemical similarity with piperidine, which is found in the black pepper plant [4]. The chair conformation of N–H bond occupies the crystallographic inversion centre in the equatorial position. The piperazine core has primarily two nitrogen atoms to enhance the stability for hydrogen bonding, and the combination of carboxylic acid plays an important role in the formation of complex molecules [5, 6]. However, in piperazine structure the presence of C–H bond enhances CH···π (or) CH···O interactions, which contribute to molecular packing and stabilize the crystal lattice in supramolecular structures. Thus, the ring formation of piperazine found a number of biologically active compounds [7–9]. In recent research highlights the selective RNA binding of polycationic ligands, particularly those containing piperazine [10]. Being a versatile substance, piperazine holds potential applications in both crystallographic [11] and vibrational investigations [12].

In this context, Yokozeki et al. reported the molecular structure of piperazine [13] and Jenneskens et al. described the study of various synthesis techniques for the piperazine group [14]. The normal coordinate analysis of piperazine was observed by Gunasekaran et al. [4]. Continuing the study of piperazine compounds as they are widely used in various fields due to their high nonlinear optical (NLO) efficiency. In this list of piperazine

[a] e-mails: kanagatharan.sse@saveetha.com; kanagathaara@gmail.com (corresponding author)

Published online: 14 July 2026

compounds, several researchers have shown their interest in exploring the characteristics of nonlinear optical (NLO) properties and its applications. Based on, several piperazine-based single crystals with NLO properties have been reported, such as, piperazine oxalic acid [15], 1-Acetyl-4-(4-hydroxyphenyl) piperazine [16], piperazinium isophthalate [17], and piperazinium bis(5-chlorosalicylate) [18], highlighting their potential in advanced optical technologies.

Trifluoroacetic acid (TFA) forms interesting crystalline complexes with amines and amino acids. The protonated amino acid salts have garnered interest due to their promising nonlinear optical (NLO) properties. L-arginine trifluoroacetate (LATF) and L-lysinium trifluoroacetate (LLTFA) are examples of crystals with excellent NLO properties [19, 20]. The presence of a carboxylic acid (COOH) group along with a trifluoromethyl group (-CF_3) enhances volatility, making these compounds useful in chromatography and as solvents in chemical reactions. Based on this, piperazine and trifluoroacetate are good companion materials. The present work focuses on piperazine with bis (trifluoroacetic acid). Piperazine undergoes proton transfer with trifluoroacetic acid, forming piperazinium cations. This process leads to ionic and hydrogen bonding with trifluoroacetate anions. Among the detailed literature on piperazine bis (trifluoroacetic acid), the structure and experimental studies with NLO applications were reported by Sahaya et al. [21]. However, the theoretical study of these materials has not been studied. In this paper, we discuss XRD, FT-IR, and UV studies, as well as molecular electronic properties, such as HOMO–LUMO, NBO, and MEP calculations. The chemical behavior was studied through ELF & LOL, RDG–NCI, and Fukui analysis have been determined. Furthermore, the three-dimensional intermolecular interactions and 2D fingerprint plot studied by Hirshfeld surface analysis.

2 Synthesis

Piperazinium bis(trifluoroacetate) (PTFA) was synthesized by reacting piperazine and trifluoroacetic acid in a 1:2 molar ratio, using methanol solvent. Trifluoroacetic acid was gradually added to the stirred solution, and after 5 h, water was added to slightly undersaturate the solution and prevent unwanted nucleation. The solution was filtered to remove dust, then placed in a clean room to allow slow evaporation, yielding transparent single crystals. The PTFA crystal pictograph as shown in Fig. 1.

3 Computational details

PTFA is an ionic molecular crystal consisting of piperazinium cations and trifluoroacetate anions forming a 3D hydrogen-bonded crystal network. However, for DFT calculations, a single ion pair was used as a molecular model to study electronic and optical properties. The "infinite 3D structure" refers to crystal packing, not an isolated molecule. The theoretical calculations of the PTFA compound were carried out using the Gaussian 16 software package [22]. The initial molecular geometry was taken from the experimental crystal structure (CIF file), which was used as the input structure for the DFT calculations.. Full geometry optimization was then performed using density functional theory (DFT) with the B3LYP functional and the 6–311 + + G (d, p) basis set without applying any symmetry constraints. The optimization could proceed until the convergence criteria were satisfied, and the convergence was confirmed after several optimization cycles. Frequency calculations were subsequently performed at the same level of theory to confirm that the optimized structures correspond to stable minima on the potential energy surface, as indicated by the absence of imaginary (negative) frequencies. This confirms that the optimized structures are true minimum energy structures. The optimized structure was further used to obtain the bond lengths, bond angles, and vibrational frequencies. The vibrational assignments were analysed using the VEDA program [23] and visualized using Chemcraft software [24]. The molecular orbitals and electron density distributions were visualized using GaussView 5 [25]. In addition, the optimized structure was used for the calculation of electronic properties, such as NBO analysis, HOMO–LUMO energy levels, and the TD-DFT electronic absorption spectrum. Furthermore, ELF, LOL, and RDG–NCI analyses were performed using the Multiwfn program [26], and Hirshfeld surface analysis was carried out using Crystal Explorer 17 [27] to investigate intermolecular interactions and crystal packing in the PTFA compound.

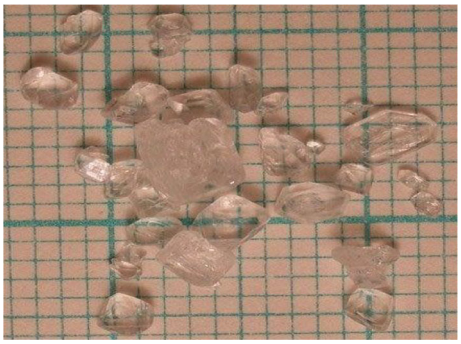

Fig. 1 Photograph of PTFA Crystal

4 Results and discussion

4.1 Structural analysis

The structural analysis of PTFA compound has been carried out on both experimental and theoretical approaches. Single crystal XRD study confirms the

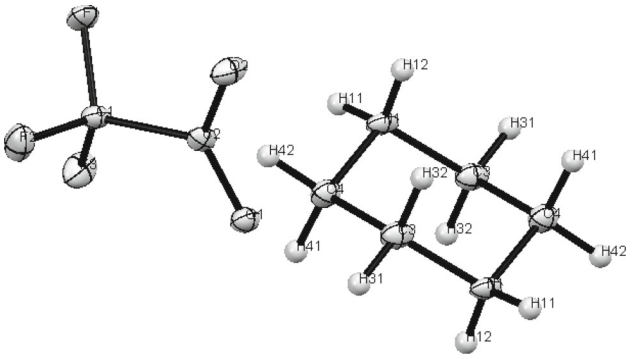

Fig. 2 ORTEP diagram of PTFA Crystal

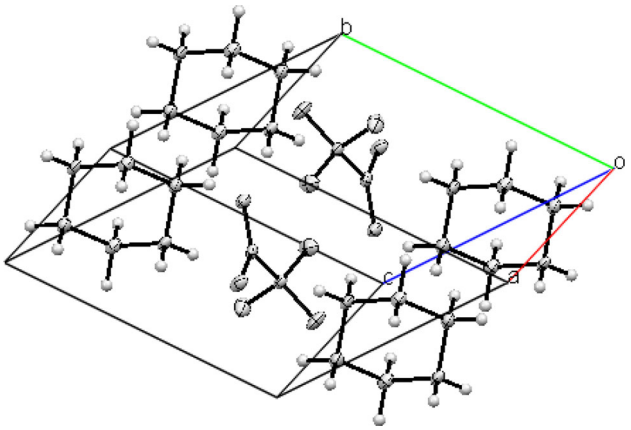

Fig. 3. 3D structure of PTFA Crystal

structure belongs to the triclinic system with P-1 space group. The calculated lattice parameters are: a = 6.1688(4) Å, b = 7.3406(5) Å, c = 7.5413(6) Å, α = 62.174(6) °, β = 88.835(4) °, and γ = 77.640(5) °, with volume of V = 293.75(4) Å^3. These results are perfectly matched with previously reported crystal structure of PTFA compound data [21].

The atomic numbering scheme of PTFA molecule as shown in Fig. 2, where the asymmetric unit consists of two independent pairs, comprising a diprotonated piperazine cation and a trifluoroacetate anion. The piperazine ring adopts a chair conformation, reinforced by crystallographic inversion symmetry. The hydrogen atoms of each amino group in cation of PTFA are hydrogen-bonded to the oxygen atoms of the carboxylate groups in the anions. For each amino group, one hydrogen atom forms a bifurcated hydrogen bond with both oxygen atoms of the carboxylate group of one anion.

This interaction, in which both oxygen atoms of each carboxylate group serve as acceptors for two hydrogen bonds, forms an intermolecular N–H$\cdots$O hydrogen bond network that links the cations and anions, resulting in an infinite three-dimensional structure (Fig. 3). In parallel, the molecular geometry of PTFA was optimized using DFT calculations. The optimized structure, as well as the bond angles and bond distances of the piperazine derivative molecule, were computed using the B3LYP/6–311 + + G (d, p) method, as illustrated in Fig. 4.

The Quantum chemical calculations yielded the minimum optimized energy of the studied compound in the gas phase, calculated to be − 1321.990431 Hartree, with the symmetry classified as the C1 point group. Table 1 shows that the observed C–N bond length matches the theoretical range of 1.491- 1.481 Å. In the piperazine ring, the bond lengths of nitrogen atoms in amino groups are notably short. The N1A–H12A bond measures 0.885 Å experimentally and 1.018 Å theoretically, with N1B–H12B exhibiting similar values.

The N1B–H11B and N1A–H11A bond distances are 0.889 Å from XRD measurements and 1.593 Å from DFT calculations, with the significant discrepancy attributed to protonation. Moreover, all C–H bonds are observed at 0.99 Å and calculated values at 1.09 Å. The C3A–C4A and C4B–C3B bonds near the amino group around 1.500 Å, are notably longer due to the presence of similar charges. The bond lengths between the C–F are around 1.3 Å, reflecting polar covalent interactions due to high electronegativity of fluorine atoms. The calculated O–H bond length is 1.043 Å, whereas the observed value is significantly longer at 2.919 Å, likely due to intermolecular interactions between the cation and anion. This suggests a correlation between the bond angles, where the N1A–H11A–O2 angle exhibits a considerable discrepancy between the experimental at 168.71° and theoretical at 178.16° values clearly reflects the influence of crystal packing. In the solid-state structure, the N–H group is involved in strong intermolecular N–H···O hydrogen bonding with the trifluoroacetate anion, which slightly distorts the bond angle from the nearly linear value obtained in the gas-phase optimized structure. Whereas the C–H–C and C–C–F bond

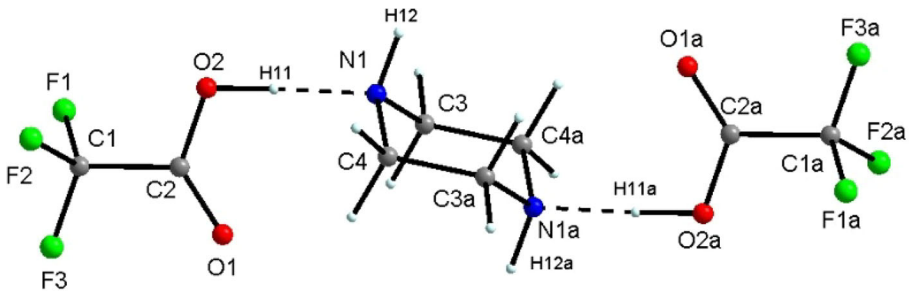

Fig. 4 Optimized structure of PTFA compound

Table 1 DFT optimized parameters for PTFA compound

Atom	Bond distance (Å)		Atom	Bond distance (Å)	
	Exp	Calculated		Exp	Calculated
N1A–C4B	1.491	1.481	C4B–C3B	1.515	1.529
N1A–C3A	1.491	1.481	C3B–N1B	1.491	1.481
N1A–H11A	0.889	1.593	N1B–H12B	0.885	1.018
N1A–H12A	0.885	1.018	N1B–H11B	0.889	1.593
C4B–H41B	0.99	1.094	N1B–C4A	1.491	1.481
C4B–H42B	0.99	1.092	C3A–C4A	1.515	1.529
C3B–H31B	0.99	1.092	C3A–H32A	0.99	1.094
C3B–H32B	0.99	1.094	C3A–H31A	0.99	1.092
C4A–H42A	0.99	1.092	H11A–O1	2.919	1.043
C4A–H41A	0.99	1.094	C1–F1	1.336	1.347
C2–O2	1.245	1.207	C1–F2	1.343	1.335
C1–C2	1.554	1.554	C1–F3	1.333	1.347
Atom	Bond Angle (°)		Atom	Bond Angle (°)	
	Exp	Calculated		Exp	Calculated
H11A–N1A–H12A	109.50	110.06	H41A–C4A–H42A	108.11	107.57
H12A–N1A–C3A	111.58	109.30	H41A–C4A–N1B	109.56	106.94
N1A–C3A–H31A	109.64	108.51	H42A–C4A–N1B	109.58	108.51
N1A–C3A–H32A	109.64	106.94	H11B–N1B–H12B	109.50	110.04
C3A–H32–C4A	109.64	110.56	H11B–N1B–C3B	109.70	108.31
C3A–C4A–H41A	109.58	110.57	H12B–N1B–C3B	111.58	109.29
C3A–C4A–H42A	109.55	110.42	N1B–C2B–H32B	109.64	106.94
H42B–C4B–H41B	108.11	107.57	H31B–C3B–N1B	109.64	108.51
N1A–C4B–H42B	109.58	108.51	H32B–C3B–C4B	109.64	110.56
N1A–H11A–O2	168.71	178.16	C3B–C4B–H41B	109.58	110.57
C4A–N1B–C4B	111.21	111.52	C3A–N1A–C4B	111.21	111.52
O2–C2–O1	129.73	127.65	C2–C1–F1	110.16	110.70
O2–C2–C1	113.23	110.96	C2–C1–F2	110.09	110.72
O1–C2–C2	117.00	121.38	C2–C1–F3	110.30	110.12

angles closely match the observed and calculated values. The C–H–C bond angle is 109°, closely aligning with the calculated 110°, with a slight deviation from the ideal tetrahedral angle, and the C–C–F angle is approximately 110° for both XRD and DFT values. However, the values of the bond distances and angles show a good agreement with minor deviations between the XRD data and DFT calculations. The slight variations observed in certain bond lengths and bond angles can be attributed to crystal packing effects. In the crystalline state, the diprotonated piperazinium cation and the trifluoroacetate anion are strongly connected through intermolecular N–H···O hydrogen bonds, forming an extended three-dimensional hydrogen-bonded network. These intermolecular interactions influence the molecular geometry, whereas the optimized structure corresponds to an isolated molecule in the gas phase and the experimental structural parameters were obtained from the solid-state crystal structure.

4.2 Hirshfeld analysis

The crystalline surface packing was used to identify the stability and overall arrangement of the crystal structure. The technique of Hirshfeld surface (HS) analysis was carried out to obtain a relationship between the intermolecular interaction of the molecule [28]. This method provides detailed information about the non-covalent interactions (hydrogen bonds, van der Waals forces, and π–π stacking). In the Hirshfeld surface analysis, the regions of PTFA molecular surface are mapped, based on $d_{norm,}$ which is determined by d_e (the distance to the nearest external nucleus) and d_i (the

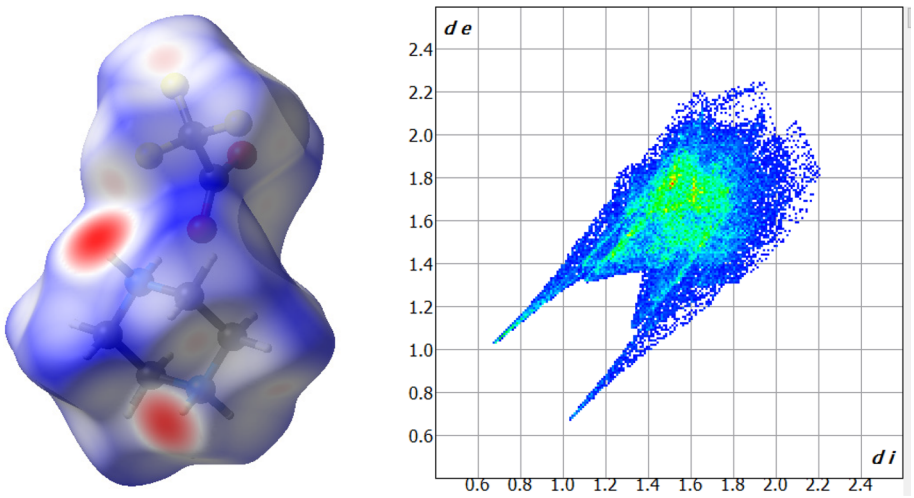

Fig. 5 Overall Mapped surface area of PTFA crystal

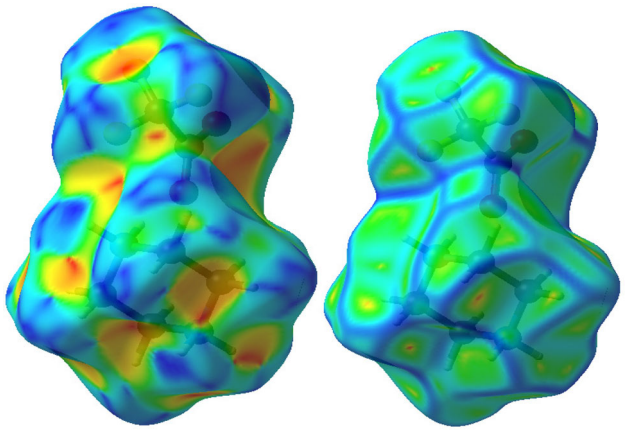

Fig. 6 Shape index and curvedness image of PTFA

distance to the nearest internal nucleus). The ranges of d_{norm} (− 0.7002 to 1.116 Å), d_e (0.6763 to 2.2680 Å) and d_i (0.6758 to 2.2064 Å). These contour surfaces are visualized in various colour codes to show their interactions with neighboring molecules.

To red (close contact), blue (longer than typical distances) and white (van der Waals distance) are used to identify the strength and nature of the crystal. The circular depressions (deep red) on the PTFA surfaces indicate close hydrogen bonding interactions as shown in Fig. 5. The HS-mapped surface with a shape index (Fig. 6) shows complementary pairs of hollows (in red) and bumps (in blue), indicating the presence of π–π stacking. The root mean square curvature determines a surface's curvature (Fig. 6), which can be observed when comparing a large green area (flat) to a dark-blue edge (with noticeable curvature).

In addition, the total HS surface area was also generated 2D-fingerprint regions to determine the percentage contributions of intermolecular interactions occurring in the molecule [29]. By utilizing the crystal explorer software to view the intermolecular interactions of PTFA compounds.

Thus, the two-dimensional plots of PTFA compound indicate F···H interactions (Fig. 7) have the highest contribution to the crystal packing (42.9%). The next major contribution occurred between O···H interactions (33.6%). The proportions of other intermolecular interactions are as follows: H···H (8.2%), F···O (6.7%), F···F (5.1%), and F···C (1.5%) as mentioned in Fig. 6. In this Hirshfeld analysis the strength of crystal packing influences the mechanical stability of the PTFA compound. To assess the mechanical stability of the compound, a void analysis was conducted to calculate voids in the crystal packing. This void calculation involved summing the electron densities of all atoms in the asymmetric unit, assuming spherical symmetry. The void surface, an isosurface of procrystal electron density, was calculated for the unit cell, intersecting the boundary and enclosed by capping faces to define the void volume. The calculated volume of crystal voids is 207.06 Å3, with 10.94% free space in the unit cell. Hence, the results for this compound indicates the crystal packing appears compact, and the mechanical stability should be substantial.

4.3 Vibrations spectroscopic analysis

The vibrational frequencies of piperazine trifluoroacetic acid (PTFA) were calculated using the B3LYP method with the basis set of 6–311 + + G (d, p). The experimental FT-IR vibrational spectrum of PTFA as shown in Fig. 8. The experimental and calculated vibrational spectroscopic frequencies were compared are listed in Table 2. There are some variations between experimental and calculated values can be attributed to factors such as anharmonicity and environmental effects. The vibrational bands observed in the range of 4000–500 cm^{-1} arise from the vibrations of protons in hydrogen bonds, as well as the internal vibrations of piperazine cations and trifluoracetic anions. The interpretation of the vibrational spectrum is challenging below 800 cm^{-1} due to fundamental, overtone, and combination bands.

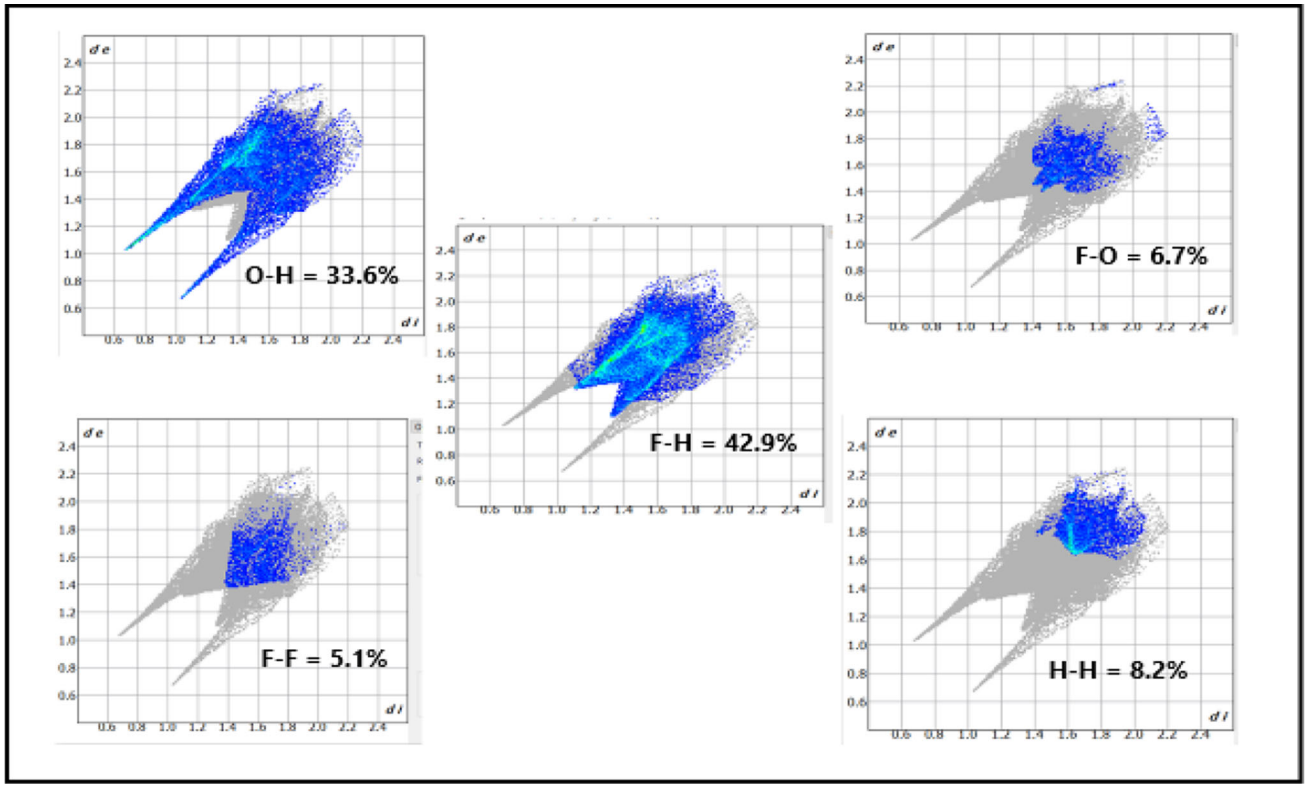

Fig. 7. 2D finger plots of PTFA

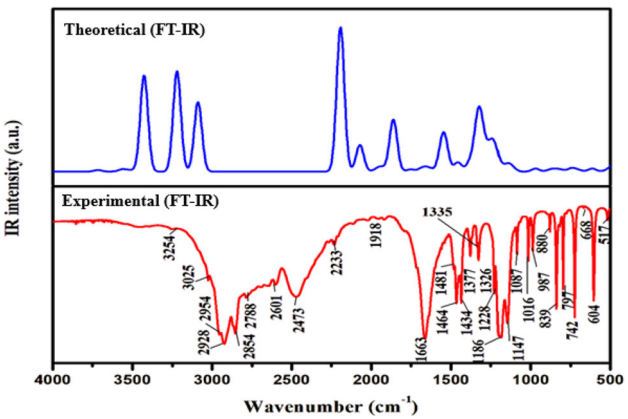

Fig. 8 FT-IR spectrum of PTFA

4.3.1 Vibrations of piperazine cation

Amino groups are generally electron-donating in nature, and their stretching vibrations usually appear in the region 3500–3100 cm^{-1} [30]. In the present compound, the N–H stretching vibration is observed at 2854 cm^{-1} in the experimental spectrum, while the calculated value appears at 3009 cm^{-1}. The shift toward lower wavenumber in the experimental spectrum indicates that the N–H bond is involved in strong intermolecular hydrogen bonding, which weakens the bond strength and reduces the vibrational frequency. The O–H stretching vibration is identified at 2788 cm^{-1} experimentally and at 2719 cm^{-1} in the theoretical spectrum, showing good agreement between the experimental and computed results. The reduced frequency further confirms the presence of strong hydrogen-bonding interactions in the crystal structure. The C–H stretching vibrations normally occur in the region 3100–3000 cm^{-1} [31, 32]. In this compound, the important experimental bands are observed at 3254 and 3025 cm^{-1}, while the corresponding calculated values appear at 3257 and 3037 cm^{-1}, showing very close agreement. The higher-frequency band around 3254–3257 cm^{-1} shows a slight shift toward higher wavenumber, which may be attributed to the combined contribution of C–H and N–H vibrations in the piperazinium ring along with the intermolecular interactions present in the crystal lattice. The CH_2 bending vibrations are generally observed in the region 1500–800 cm^{-1}[33]. In the present study, the major calculated bands appear at 1490 and 1466 cm^{-1}, while the experimental bands are observed at 1481 and 1464 cm^{-1}, showing good agreement. These small deviations arise mainly from hydrogen bonding and electrostatic interactions between the piperazinium cation and the trifluoroacetate anion.

Table 2 The B3LYP/6–311 + + G (d, p) calculated frequencies (ν_{calc}), scaled frequencies (ν_{sc}), mode assignments PED, experimental frequencies for IR spectrum (ν_{exp}.IR) and assignments of PTFA compound

Unscaled	Scaled	Vib., Mode No. (PED)	Exp.FT-IR (cm^{-1})	Assignment descriptions
3257	3143	CH, s7(28); CH, s8(72)	3254	υ(C–H)
3188	3076	CH, s11(63); CH, s12(37)		υ(C–H)
3141	3031	CH, s5(39); CH, s6(59)	3025	υ(C–H)
3124	3014	CH, s7(71); CH, s8(28)		υ(C–H)
3095	2986	CH, s9(28); CH, s10(57); CH, s5(12)		υ(C–H)
3086	2978	CH, s11(36); CH, s12(62)		υ(C–H)
3082	2974	CH, s6(38); CH, s10(11); CH, s5(47)	2954	υ(C–H)
3037	2930	CH, s9(69); CH, s10(30)		υ(C–H)
3009	2904	NH, s3(94)	2854	υ(N–H)
2832	2733	FH, s1(88)	2788	υ(H–F)
2719	2624	OH, s2(85)		υ(O–H)
1951	1883	OH, s4(51); OC, s18(22)	1918	υ(O–H)
1847	1782	OC, s17(85)		υ (C=O)
1758	1696	NC, s20(64); HNC, s40(15)		υ(C–N)
1732	1671	NC, s19(82); HCH, s48(11)	1663	υ(C–N)
1667	1609	OH, s4(19); OC, s18(48)		υ (O–H); υ(C=O)
1574	1519	NC, s20(11); HNC, s40(45); HCH, s45(24)	1481	υ(C–N); δ (C–H)
1518	1465	OC, s21(28); CC, s33(10); FHO, s37(20); HOC, s41(22)	1464	υ(C–C)
1501	1449	HCH, s48(71)		δ (C–H)
1490	1438	HCH, s42(66); HCNC, s74(10)	1434	δ (C–H) C–N
1475	1423	NC, s20(15); HCH, s45(63)		δ (C–H)
1466	1415	HCH, s46(91)		δ (C–H)
1410	1361	OC, s21(17); FHO, s37(14)	1377	δ(C–H); δ(C–O)
1406	1357	HCN, s43(11); HCN, s47(28)		δ(C–N)
1393	1344	OC, s22(19); CC, s32(10); OHF, s39(16); COH, s58(21)		υ (C=O)
1383	1334	HCH, s42(13); HCNC, s74(27); HCNC, s75(25)	1326	δ (C–H)
1329	1283	HCN, s43(14); HCN, s44(13)		υ(C–C)
1318	1272	OC, s22(13); CC, s32(10); OHF, s39(19); HCN, s43(10); COH, s58(18)		υ(COO)

4.3.2 Vibrations of trifluoroacetate anion

The C=O stretching vibration of the trifluoroacetate group is generally observed near 1700 cm^{-1}, reflecting the strong electron-withdrawing effect of the fluorine atoms attached to the carboxylate group. In the present compound, the important infrared band corresponding to the carbonyl group appears at 1918 cm^{-1} experimentally, while the calculated value is obtained at 1883 cm^{-1}, showing good agreement between the experimental and theoretical results. The COO^- asymmetric stretching vibration usually occurs in the region 1550–1610 cm^{-1}, whereas the symmetric stretching vibration is found in the range 1300–1420 cm^{-1} [34, 35].

In this PTFA compound, the asymmetric stretching band is observed at 1663 cm^{-1} in the experimental spectrum and the calculated spectrum at 1609 cm^{-1}. Similarly, the symmetric stretching vibration is clearly identified at 1326 cm^{-1} experimentally and at 1283 cm^{-1} theoretically, confirming the presence of the trifluoroacetate anion in the crystal structure.

The strong electron-withdrawing nature of the fluorine atoms also gives rise to intense C–F stretching vibrations. For the selected PFTA compound, the most important bands are observed at 1228 cm^{-1} &

Table 2 (continued)

Unscaled	Scaled	Vib., Mode No. (PED)	Exp.FT-IR (cm^{-1})	Assignment descriptions
1283	1238	HCHF, s78(55)	1228	δ (C–H)
1263	1219	HCN, s49(52)		δ (C–H)
1249	1205	FHOC, s82(76)		
1213	1171	FC, s23(57)	1186	δ (C–F)
1205	1162	FC, s25(48)		δ (C–F)
1201	1159	HCN, s44(30); HCN, s49(11)		δ (C–H)
1193	1151	FC, s24(46); FCF, s63(14)	1147	δ (C–F)
1169	1128	OHN, s52(13); HNCH, s72(60)		δ (C–H)
1162	1122	OC, s22(21); FC, s26(36); FCF, s62(10)		δ(C–O)
1141	1101	FC, s27(57)		δ (C–F)
1130	1091	HCNC, s76(55); HCHF, s77(18)		δ(C–N)
1125	1085	FHN, s36(31); FHNC, s70(11)	1087	δ(C–N)
1121	1082	FC, s26(10); FC, s28(41)		δ (C–F)
1106	1067	HCHF, s80(12); HCNC, s81(52)		δ(C–N)
1076	1039	FHN, s36(14); HCN, s47(10)		δ (C–H)
1053	1016	FHN, s36(20); FHNC, s70(14)	1016	δ(C–N); δ(C–H)
1036	1000	OHFF, s71(21); COHF, s89(31); CCOH, s94(18)		δ (C–F)
1032	995	NC, s29(25); CC, s31(26)		δ(C–N); υ(C–C)
1019	984	NC, s30(16); CC, s31(24)	987	δ (C–N); υ(C–C)
903.7	872	FF, s34(97)	880	υ (F–F)
890.5	859	NC, s29(24); NC, s28(31)	839	δ (C–N)
837.4	808	NC, s29(14); NC, s30(24); CC, s31(16)		υ (C–C); υ(C–N)
826	797	FC, s24(11); FC, s25(12); FC, s27(13); CC, s33(19); OCO, s57(26)	797	δ (C–F)
810.3	782	FC, s23(10); FC, s26(12); FC, s28(15); CC, s32(17); OCO, s53(29)		δ (C–F)
794.7	767	FCFC, s99(15); COOC, s102(65)		δ (COO)
770.6	744	OCOC, s97(64); FCFC, s101(17)	742	δ (COO)
716.8	692	OCO, s57(25); FCF, s60(13); FCF, s61(10); FCF, s63(13)		δ (C–F)
707.2	682	OCO, s53(33); FCF, s59(12); FCF, s62(11); FCF, s64(13)		δ (COO)
693.1	669	HCHF,s77(13);HCNH,s79(11);HCHF,s80(11)	668	δ (C–F)

1186 cm^{-1}, which are in good agreement with the calculated values near 1238 cm^{-1} & 1171 cm^{-1}. These strong peaks clearly indicate the presence of the trifluoroacetate group. In addition, the deformation vibrations of the trifluoroacetate anion are observed in the lower wavenumber region. The important bands appearing at 797 cm^{-1} & 517 cm^{-1} correspond to the bending vibrations of the COO^- group, while the peak observed near 880 cm^{-1} in the experimental spectrum, with a calculated value close to 872 cm^{-1}, further confirms the presence of the fluorine-containing trifluoroacetate anion. These small deviations between experimental and theoretical values mainly arise due to strong intermolecular hydrogen bonding and electrostatic interactions present in the PTFA crystal lattice.

4.4 HOMO–LUMO analysis

The frontier molecular orbitals of the compound are the "frontier" of electron occupation. The highest occupied molecular orbital (HOMO) and lowest unoccupied molecular orbital (LUMO) determine the interaction between the molecules. The energies of HOMO–LUMO were theoretically evaluated using the B3LYP/6–311 + + G (d, p) technique.

The values of energy gap determine the optical & chemical reactivity of the molecule [36, 37].

Table 2 (continued)

Unscaled	Scaled	Vib., Mode No. (PED)	Exp.FT-IR (cm^{-1})	Assignment descriptions
668.1	645	HCHF,s77(13);HCHF,s80(24);HCNC,s81(11)		δ (C–F)
597.7	577	FC,s25(12);FCF,s63(13);CCO,s68(22);FCFC,s98(32)	604	δ (COO)
589.2	569	FC,s23(12);FCF,s62(13);CCO,s67(19);FCFC,s100(30)	517	δ (COO)
519.3	501	CC,s31(10);HNC,s51(14);CCN,s66(10);HCHF,s77(15);HCHF,s80(10)		δ (C–F)
517.9	500	FCF,s60(47);FCF,s61(25);		δ (C–F)
514	496	FCF,s59(36);FCF,s64(38)		δ (C–F)
479.6	463	FCF,s61(11);FCF,s63(12);FH,s13(15);CNC,s56(18)		δ (C–F)
457.8	442	FH,s13(11);CNC,s56(35);	446	δ (C–N)
432	417	FCF,s59(10);FCF,s62(32);FCF,s64(10);CCO,s67(20)		δ (C–F)
425.4	410	CC,s33(22);OCO,s57(10);FCF,s63(23)	412	δ (COO)

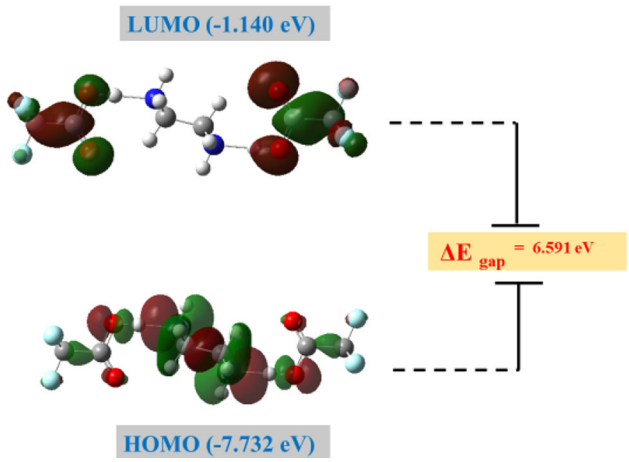

Fig. 9 HOMO—LUMO plot of PTFA

Table 3 Calculated energy band gap & global reactivity parameters of the PTFA compound

Parameters	Formula	Gaseous Phase (eV)
HOMO	E_{HOMO}	− 7.732
LUMO	E_{LUMO}	− 1.140
Energy gap ΔE	E_{HOMO}—E_{LUMO}	6.591
Ionization potential (A)	− E_{HOMO}	7.732
Electron affinity (I)	− E_{LUMO}	1.141
Electronegativity (χ)	(I + A)/2	4.436
Global hardness (η)	(A-I)/2	3.295
Global softness (S)	1/2η	1.647
Chemical potential (μ)	− χ	− 4.436
Global electrophilicity (ω)	$\mu^2/2\eta$	2.986
Maximum electronic charge (ΔN max)	− (μ/η)	1.3462

The HOMO is logically viewed as nucleophilic or electron donating, while the LUMO is electron acceptor. The simulated HOMO & LUMO plots are depicted in Fig. 9, where positive (green) and negative (red) phases represent the charge transfer within the molecule. Meanwhile the π nature HOMO is delocalized over the piperazine ring and LUMO is primarily localized in the trifluoroacetate anion portions. In this case, the HOMO orbital has a large number of electrons with the energy − 7.732 eV donating electrons to the LUMO orbital having few electrons with the energy − 1.140 eV. The energy gap (ΔE) is 6.591 eV, the large energy gap reveals the chemical stabilization of the PTFA compound. Using HOMO & LUMO values, the global molecular reactivity descriptors such as electronegativity, chemical hardness, softness, chemical potential and electrophilicity index were calculated and are listed in Table 3.

The energies of the HOMO & LUMO orbitals of the molecule correspond to its ionization potential (I) and electron affinity(A) [15]. The value of ionization potential corresponds to 7.732 eV, it indicates the energy required to remove an electron from the highest occupancy. The lower A of 1.140 eV shows that the compound readily accepts electrons, suggesting higher reactivity with nucleophiles. The higher hardness (3.295 eV) and lower softness values (1.647 eV) confirms the higher molecular hardness associated with the PTFA molecule. However, the electronegativity (χ) denotes the ability of an atom or group of atoms to attract electrons towards itself. The calculated value of electronegativity (χ) is 4.436 eV. The chemical potential (μ) describes the chemical stability and reactivity of chemical compounds. The chemical potential (μ) is − 4.436 eV, indicating high stability and polarizability of the molecule. Electrophilicity describes the electrophilic strength of a molecule and it indicates the propensity or capacity to accept electrons. The global electrophilicity index (ω)

Table 4 Second-order perturbation theory analysis of the Fock matrix in NBO basis calculated at B3LYP/6–311 + + G (d, p) level

Donor(i)	Acceptor(j)	E (2) (Kcal/mol)	E(j)-E(i) (a.u.)	F (i,j) (a.u)
σ(O5–H25)	σ*(C6–C7)	4	1.01	0.058
σ(C12–H13)	σ*(C18–H20)	2.54	0.91	0.043
σ(C12–H14)	σ*(C9–N24)	3.48	0.83	0.043
σ(C12–H14)	σ*(N15–C18)	3.75	0.83	0.05
σ(C21–H22)	σ*(N15–H17)	3.03	0.89	0.046
σ(C6–C7)	σ*(O5–H25)	2.95	1.01	0.05
LP (2)–F1	σ*(F3–C6)	6.31	0.68	0.059
LP (2)–F1	σ*(C6–C7)	6.58	0.71	0.062
LP (3)–F1	σ*(F2–F6)	12.43	0.66	0.081
LP (3)–F1	σ*(F3–C6)	7.92	0.68	0.066
LP (2)–F2	σ*(F3–C6)	6.31	0.68	0.059
LP (2)–F2	σ*(C6–C7)	6.59	0.71	0.062
LP (3)–F2	σ*(F1–C6)	12.44	0.66	0.081
LP (3)–F2	σ*(F3–C6)	7.92	0.68	0.066
LP (2)–F3	σ*(C6–C7)	7.52	0.71	0.066
LP (3)–F3	σ*(F1–C6)	11	0.66	0.077
LP (3)–F3	σ*(F2–C6)	10.99	0.66	0.076
LP (2)–O4	σ*(O5–C7)	26.51	0.69	0.123
LP (2)–O4	σ*(O6–C7)	25.87	0.55	0.107
LP (1)–O5	σ*(O4–C7)	9.94	1.19	0.097
LP (2)–O5	π*(O4–C7)	60.65	0.32	0.125
LP (1)–N24	σ*(O5–H25)	48.5	0.68	0.164
LP (1)–N15	σ*(H16–O30)	48.88	0.68	0.165
LP (3)–F26	σ*(F27–C31)	12.43	0.66	0.081
LP (3)–F26	σ*(F28–C31)	7.92	0.68	0.066
LP (3)–F27	σ*(F26–C31)	12.43	0.66	0.081
LP (2)–O30	π*(O29–C32)	60.7	0.32	0.125

is defined in relation to chemical potential and chemical hardness. Based on these, PTFA compound has the lower chemical potential and higher electrophilicity index values identified are comparable with that of the bioactive molecules.

4.5 NBO analysis

Studies of charge transfer and conjugative interactions in molecular systems are analyzed by the Natural Bond Orbital (NBO) program. It provides insights into electron delocalization and bonding characteristics. By the NBO analysis the inter and intramolecular atoms interaction were studied [38]. The NBO analysis reveals a molecular stability, reactivity, and electronic properties to explain the hyperconjugative effects and donor–acceptor interactions within the molecule. This method determines the most accurate natural Lewis structure by maximizing electron density localization. Using the second order Fock matrix to evaluate the donor acceptor interaction and exchanges between donor–acceptor orbitals of a molecule. For each donor (i) and acceptor (j), the stabilization energy E (2) related to the delocalization terms i and j is given by,

$$E_2 = \Delta E_{ij} = \frac{q_i(F_{i,j})^2}{(E_i - E_j)} \quad (1)$$

where, E_i and E_j are energies of Lewis and non-Lewis NBO's F (i, j) is the off-diagonal NBO Fock matrix component, and q_i is the population of donor orbital occupancy [39].

The intensity of interaction between donors and accepters increases with increasing E (2) values. The values of occupancy and stabilization energy were extracted from the NBO Gaussian output and values are given in Table 4.

The results from the PTFA compound indicated interactions between lone pair (LP) donor orbitals and antibonding orbitals. Specifically, intermolecular interactions occurred between LP (2)-N24 → π*(O5–H25) and between LP (2)-N15 → π*(H16–O30), with respective stabilization energies *E* (2) of 48.5 and 48.8 kcal/mol. A stronger interaction was observed

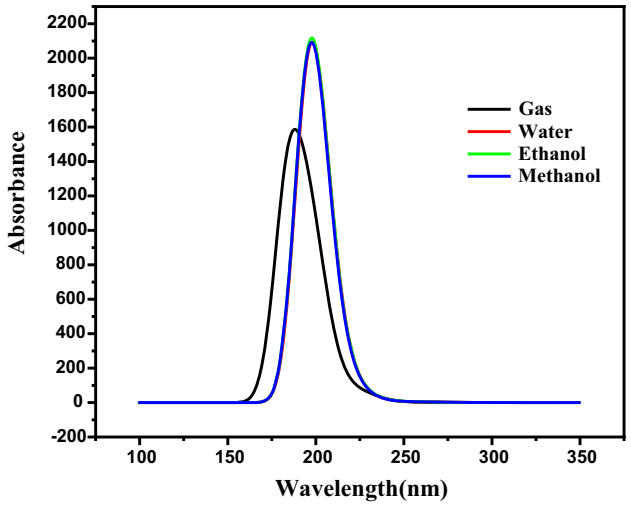

Fig. 10 Absorption spectrum of PTFA compound

between LP (2)-O5 → π*(O4–C7) and between LP (2)-O30 → π*(O29–C32), which exhibited the highest perturbation energies among all the interactions, with values of 60.7 and 60.65 kcal/mol, respectively. The second-order hyperconjugation interactions bonding to antibonding that is σ(C21–H22) → σ*(N15–H17) and σ(C12-H14) → σ*(N15–C18), exhibiting the stabilization energies 3.03 and 3.75 kcal/mol. It transfers the electron density from C–H bonding to antibonding (σ*) orbitals near nitrogen atoms in the piperazine ring. Thus, the interactions in the Piperazine and its derivatives highlights their crucial role in enhancing molecular stability, influencing reactivity, and determining overall properties.

4.6 Ultraviolet–visible analysis

To understand the electronic transitions of the PTFA compound, TD-DFT/6–311 + + g (d, p) basis set method was performed [40, 41]. The simulated spectra were compared with gaseous and three polar solvent (water, methanol and ethanol) phases. The calculated UV absorption maxima (λ_{max}) are related to electron availability. The absorption spectrum of PTFA compound shows a spectral range that extends the UV region from 100 to 350 nm (as shown in Fig. 10).

From the calculated results (Table 5), three major absorption bands were observed in all phases. The transition was influenced by the presence of conjugated systems and lone pairs in piperazine derivative, representing the excitation of electrons to higher energy levels. The λ_{max} is a function of substitution, the stronger than donor character of the substitution the more electrons pushed into the molecule, the larger λ_{max} values may be slightly shifted by solvent effects. In the gas phase, the first intense transition appears at 361.37 nm with an oscillator strength of 0.0026, which arises purely from the HOMO → LUMO (100%) transition.

The second and third transitions at 320.83 & 309.89 nm originate mainly from H-1 → LUMO and H-2 → LUMO excitations, indicating that the electronic transitions are dominated by frontier molecular orbitals. When solvent effects are included, a slight shift in the absorption maxima is observed. In water, methanol, and ethanol, the first transition appears at 378.86, 376.73 and 375.65 nm, respectively, and in all these phases the transition contribution remains HOMO → LUMO (99%). Similarly, the second and third absorption bands in the solvent phases (around 336 nm and 322 nm) are mainly contributed by H-1 → LUMO and H-2 → LUMO (≈99%) transitions. This clearly indicates that the nature of the electronic transitions does not change in different solvent environments, but only a slight bathochromic shift is observed. The transitions are mainly influenced by the presence of lone-pair electrons and the conjugated system present in the piperazinium framework, which promotes electron excitation from the HOMO to the LUMO level. The small red shift observed in the solvent phases compared to the gas phase suggests that polar solvents slightly stabilize the excited state through weak hydrogen-bonding interactions, resulting in minimal solvatochromism variation. The slight redshift in the solvent phase compared to the gas phase indicates the increased solvent polarity shifts of absorption to higher wavelengths. This specific wavelength corresponds to n → π* transitions, demonstrating a blue shift of PTFA molecule. Hence, the solvent-induced shift shows the changes in the electronic environment of PTFA compound and its interactions with solvents, particularly through the stabilization of excited states.

4.7 Fukui calculations

The local reactivity of all atoms in the studied PTFA compound was examined using the Fukui function at the B3LYP/6-311G + + (d, p) level of theory. The calculation of the Fukui function in a molecule is a valuable method for characterizing the reactive sites of chemical species [42, 43]. The Fukui function identifies the preferred regions in a molecule where the electron density is most likely to change when the number of electrons is altered. It reflects the molecule's tendency to deform its electron density at specific positions when accepting or donating electrons. By analyzing these mathematical functions, we can identify the region of nucleophilic & electrophilic molecules. It possesses the additional property, which means the total sum of the Fukui functions for all atoms in a molecule equals one. The nucleophilic, electrophilic and radical function of Fukui defined as,

$$f\left(k^{+}\right) = [q\,(N\ +1) - q\,(N)] \text{ for nucleophilic attack} \quad (1)$$

$$f\left(k^{-}\right) = [q\,(N) - q\,(N\ -1)] \text{ for electrophilic attack} \quad (2)$$

$$f\left(k^{0}\right) = \tfrac{1}{2}[q\,(N\ +1) - q\,(N\ -1)] \text{ for radical attack} \quad (3)$$

Table 5 Excited energy state from the DOS spectrum

Energy (cm^{-1})	Wavelength (nm)	Osc. Strength	Major contribs & Minor contribs
Gas			
27,672.0759	361.375129	0.0026	HOMO- > LUMO (100%)
31,168.48935	320.8368518	0.0017	H-2- > LUMO (24%), H-1- > LUMO (74%)
32,268.6296	309.8985028	0.0027	H-2- > LUMO (73%), H-1- > LUMO (25%)
Water			
26,394.49369	378.8669	0.0021	HOMO- > LUMO (99%)
29,728.7897	336.3742723	0.0032	H-1- > LUMO (99%)
30,944.26722	323.1616353	0.0037	H-2- > LUMO (99%)
Methanol			
26,543.70626	376.7371407	0.0021	HOMO- > LUMO (99%)
29,698.14063	336.7214172	0.0032	H-1- > LUMO (99%)
31,018.47023	322.3885616	0.0036	H-2- > LUMO (99%)
Ethanol			
26,620.32893	375.6527587	0.0021	HOMO- > LUMO (99%)
29,680.39643	336.9227235	0.0033	H-1- > LUMO (99%)
31,055.57173	322.0034101	0.0037	H-2- > LUMO (99%)

whereas, N, N-1, and N + 1 represent the total number of electrons in the neutral, anionic, and cationic states of PTFA compound, respectively. These values are listed in Table 6. The negative values in the Fukui function indicate regions where nucleophilic attack is less likely, suggesting these sites are not favorable for electron donation. Moreover, softness is related to accommodate electron density. For the present molecule, the electrophilicity and global softness is utilized by FMO theory [36]. From Table 6, the chemical species with the largest values of Fukui function shows high reactivity for corresponding attacks. In the title compound, the order of reactive sites electrophilic attack is 8H > 17H > 10H > 19H > 23H > 16H > 25H > 15N > 24N > 11H. For the calculated nucleophilic attack, the order is 29O > 4O > 25H > 16H > 23H > 19H > 10H > 14H > 17H > 8H. From the fukui calculations the nucleophilic attack exhibits the highest reactivity and is making the most favorable reaction due to a stronger attraction to electron-rich nucleophiles. This strong nucleophilicity enhances interactions with electron-rich biological targets, increasing biological activity.

4.8 Topological analysis

To explore the relationships between electrical and geometric structures and better to understand the bond dynamics at reactive sites on molecular surfaces, the electron localization function (ELF) and localized orbital locator (LOL) are widely used. The both analyses (ELF & LOL) are primarily to explain the covalent bond surfaces and to determine the concentration of electron density in compounds [44]. However, the ELF originates from electron pair density, while LOL displays the gradient of localized orbitals and is exploited when localized orbitals overlap.

Topological studies of the surface were attained using ELF relief maps and LOL maps. The color-filled contour maps of ELF and LOL were obtained from the Multiwavefunction program as shown in Fig. 11. From the simulated graphs, red indicates areas with high ELF and LOL values, while blue denotes regions with low ELF and LOL values [45]. On seeing the ELF relief map is scaled between 0.0 and 1.0, with delocalized electrons projected in the lower range (< 0.5). When electron density is dominated by the positions of localized electrons, LOL values are found in the upper range (> 0.5). In the PTFA molecule, all the hydrogen atoms are surrounded by red color. The core regions around the C–H and N–H chemical bonds (0.8–0.9) are characterized by circular localization domains with high values (≈1). Thus, both bonds have a covalent character with high electron localisation, and this characteristic of shared electron (covalent) bonding. In the LOL map, as it is clear from that red color, it intrudes into interstitial space between boundary atoms. The regions on red to yellow areas (C7 & H25) and (N24 & H8) can be observed at nitrogen and carbon atoms represent covalent regions with high LOL values. The ring over yellow with the green color denotes that the molecule has moderate values and has medium localization between the inner and valence layers. Hence the maps of ELF and LOL provide a clear view of electron distribution and bonding in the PTFA molecule. These insights are crucial for applications in molecular design and drug development.

Table 6 Fukui function and local softness of PTFA compound

Atoms	Mulliken atomic charges			Fukui functions			Global softness			Electrophilicity		
	N(0,1)	N-1(− 1,2)	N + 1(1,2)	Fr +	Fr-	Fr0	sr + fr +	sr-fr-	sr0 fr0	wfr +	wfr-1	w0fr0
1F	− 0.111	− 0.118	− 0.078	0.03	0.01	0.04	0.011	0.003	0.013	0.22	0.015	0.078
2F	− 0.111	− 0.118	− 0.078	0.03	0.01	0.04	0.011	0.003	0.013	0.22	0.015	0.078
3F	− 0.108	− 0.119	− 0.08	0.03	0.01	0.039	0.009	0.004	0.013	0.214	0.02	0.076
4O	− 0.208	− 0.182	− 0.160	0.05	− 0	0.023	0.016	− 0.01	0.008	0.125	− 0.05	0.044
5O	− 0.31	− 0.323	− 0.259	0.05	0.01	0.064	0.017	0.005	0.021	0.351	0.025	0.124
6C	0.132	0.0226	0.153	0.02	0.11	0.131	0.007	0.037	0.043	0.718	0.201	0.254
7C	0.064	0.111	0.066	0	− 0	− 0.045	5E-04	− 0.02	− 0.02	− 0.25	− 0.09	− 0.088
8H	0.280	− 0.150	0.332	0.05	0.43	0.483	0.017	0.143	0.16	2.649	0.785	0.937
9C	− 0.302	0.713	− 0.334	− 0	− 1	- 1.048	− 0.01	− 0.34	− 0.35	− 5.75	− 1.85	− 2.034
10H	0.197	− 0.516	0.264	0.07	0.71	0.781	0.022	0.237	0.259	4.285	1.3	1.516
11H	0.216	0.084	0.263	0.05	0.13	0.179	0.016	0.044	0.06	0.984	0.241	0.348
12C	− 0.302	0.717	− 0.335	− 0	− 1	- 1.053	− 0.01	− 0.34	− 0.35	− 5.77	− 1.86	− 2.043
13H	0.216	0.083	0.263	0.05	0.13	0.18	0.016	0.044	0.06	0.989	0.242	0.35
14H	0.1973	− 0.518	0.264	0.07	0.72	0.783	0.022	0.238	0.26	4.296	1.303	1.52
15N	− 0.493	− 0.732	− 0.408	0.08	0.24	0.324	0.028	0.08	0.108	1.779	0.436	0.629
16H	0.638	0.549	0.625	− 0	0.09	0.075	− 0	0.03	0.025	0.414	0.162	0.146
17H	0.280	− 0.150	0.332	0.05	0.43	0.483	0.017	0.143	0.16	2.647	0.784	0.937
18C	− 0.301	0.712	− 0.333	− 0	− 1	- 1.047	− 0.01	− 0.34	− 0.35	− 5.74	− 1.85	− 2.031
19H	0.197	− 0.516	0.264	0.07	0.71	0.781	0.022	0.237	0.259	4.285	1.3	1.516
20H	0.216	0.084	0.263	0.05	0.13	0.179	0.016	0.044	0.06	0.985	0.241	0.348
21C	− 0.302	0.713	− 0.334	− 0	− 1	- 1.048	− 0.01	− 0.34	− 0.35	− 5.75	− 1.85	− 2.034
22H	0.216	0.084	0.263	0.05	0.13	0.179	0.016	0.044	0.06	0.984	0.241	0.348
23H	0.197	− 0.516	0.264	0.07	0.71	0.781	0.022	0.237	0.259	4.285	1.3	1.516
24N	− 0.492	− 0.731	− 0.406	0.09	0.24	0.325	0.028	0.08	0.108	1.783	0.437	0.631
25H	0.637	0.547	0.623	− 0	0.09	0.076	− 0	0.03	0.025	0.418	0.164	0.148
26F	− 0.111	− 0.118	− 0.078	0.03	0.01	0.04	0.011	0.003	0.013	0.22	0.015	0.078
27F	− 0.111	− 0.118	− 0.078	0.03	0.01	0.04	0.011	0.003	0.013	0.221	0.015	0.078
28F	− 0.108	− 0.119	− 0.08	0.03	0.01	0.039	0.009	0.004	0.013	0.215	0.02	0.076
29O	− 0.208	− 0.183	− 0.159	0.05	− 0	0.023	0.016	− 0.01	0.008	0.128	− 0.05	0.045
30O	− 0.311	− 0.324	− 0.260	0.05	0.01	0.064	0.017	0.005	0.021	0.353	0.025	0.125
31C	0.132	0.023	0.153	0.02	0.11	0.13	0.007	0.036	0.043	0.715	0.2	0.253
32C	0.064	0.111	0.0661	0	− 0	− 0.045	5E-04	− 0.02	− 0.01	− 0.25	− 0.08	− 0.087

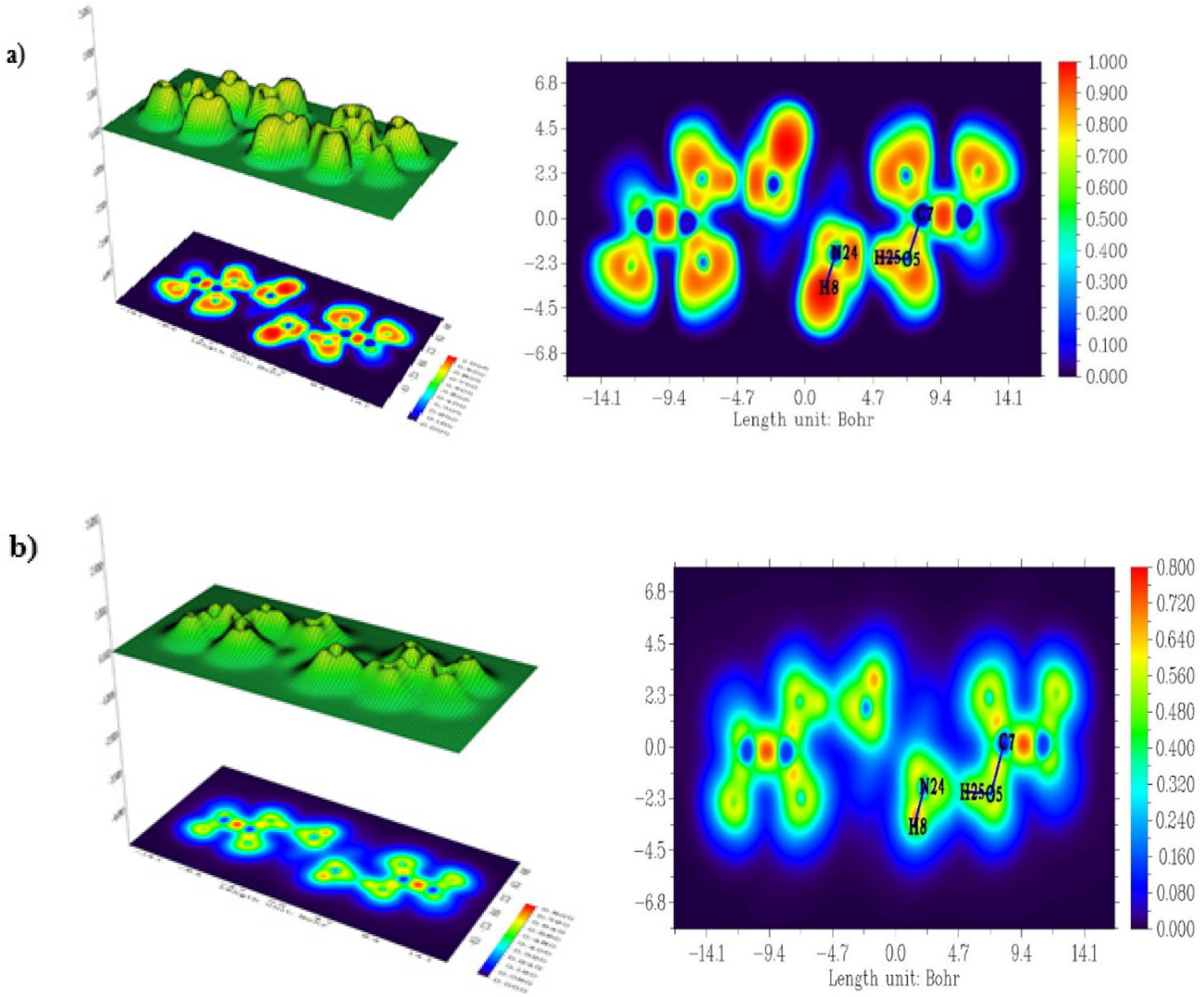

Fig. 11 **a** ELF **b** LOL image of PTFA compound

Fig. 12 NCI of PTFA

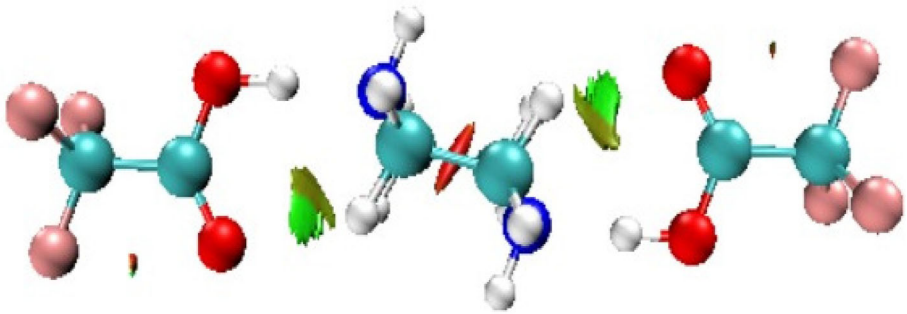

4.9 RDG-NCI analysis

To forecast real-space weak interactions through electron density, RDG analysis, a dimensionless variable was widely used [46, 47]. This method provides the regions of where non-covalent interactions are likely to occur.

RDG designed the scattered and contour graphs, with these regions often visualized using isosurface plots, colored based on the sign of the second Hessian eigenvalue (λ2). Figure 12 shows the results obtained using the VMD program, which was based on outputs from the Multiwfn software. The relationship of these interactions in the molecular structure is determined

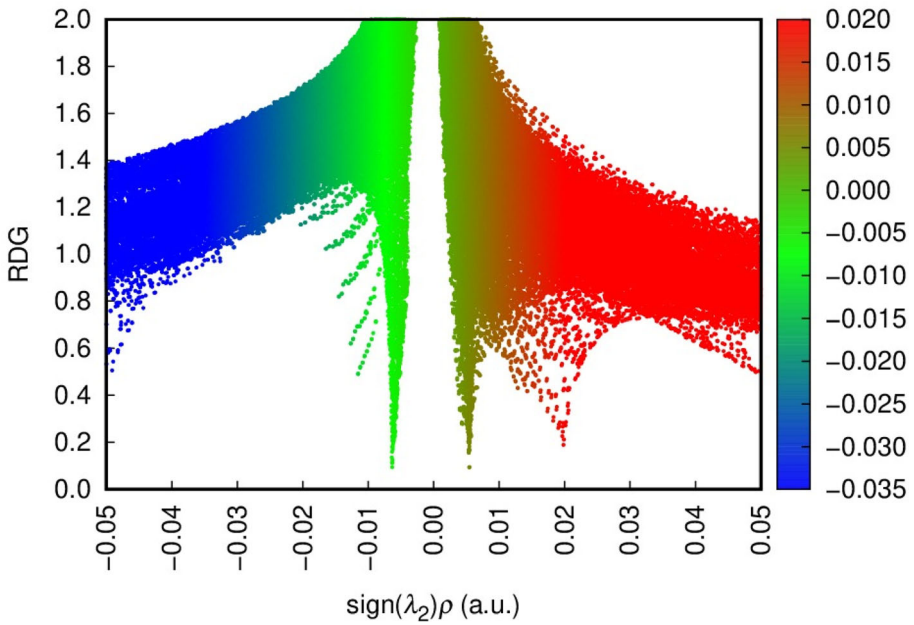

Fig. 13 2D scatter and Isosurface density of non-bonded interactions of PTFA

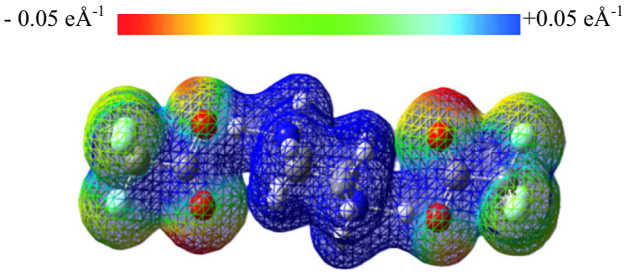

Fig. 14 Three-dimensional molecular electrostatic potential for PTFA compound

Table 7 Mulliken charge distribution of PTFA compound

Atom	Charges	Atom	Charges
F1	− 0.1107	H17	0.28017
F2	− 0.1107	C18	− 0.301
F3	− 0.1081	H19	0.19737
O4	− 0.2081	H20	0.21632
O5	− 0.31	C21	− 0.302
6C	0.1329	H22	0.21653
7C	0.06492	H23	0.19731
H8	0.28013	N24	− 0.4917
C9	− 0.3018	H25	0.63774
10H	0.19738	F26	− 0.1108
11H	0.21636	F27	− 0.1108
12C	− 0.3022	F28	− 0.1082
H13	0.2164	O29	− 0.2083
H14	0.19733	O30	− 0.3107
N15	− 0.4925	C31	0.13298
H16	0.63889	C32	0.0648

by the intensities of blue, red and green colors, representing hydrogen bonds, steric effects, and van der Waals forces, respectively. On screening the 2D plots (Fig. 13) of PTFA compound the red indicates strong repulsion (which is responsible for the steric effect) that appears in the centre of the piperazine ring system. The green colour reflects the contact between van der Walls interaction region. In the present case, the emits of green color VDW (van der Walls) was identified between the piperazine ring and trifluoroacetate atom. It denotes the non-covalent interaction that might have been liable for the labelled compound's stabilization. Therefore, through the interaction regions associated with PTFA structure, characterized by steric repulsion in the piperazine ring and van der Waals interactions between the piperazine ring and trifluoroacetate atoms, indicate that these forces are essential for stabilizing the molecular structure, thereby influencing both its geometry and packing arrangement.

4.10 MEP analysis

To understand the relative polarity of the studied compound, the Molecular Electrostatic Potential (MEP) is an effective tool to describe the molecular structure and its physicochemical property relationship [48]. This method provides a three-dimensional energy surface map to measure the charge distribution within the molecule. In general, the purpose of electrostatic potential is to identify the reactive sites of a molecule, which are crucial in drug interactions with biological molecules. Studies on the MEP surface are related to electronic density and the determination of sites for electrophilic attack, as well as nucleophilic reactions and hydrogen-bonding interactions [49, 50]. The molecular electrostatic potential projection map for PTFA is calculated using the B3LYP/6–311 + + G (d, p)

method and the MEP surface map of PTFA is shown in Fig. 14.

The reactive sites of the PTFA molecule are obtained by different colour codes.

The negative regions are coloured in red (strong repulsion), the positive regions are blue (strong attraction), and the zero potential regions are green. The maximum positive region is located at the piperazine ring, which indicates a possible site for nucleophilic attack and the negative potential sites are on electronegative oxygen atoms (O29, O30, O4 and O5). These sites provide information about the regions from which the present compound can engage in intermolecular interactions, predicting the most reactive sites for both electrophilic and nucleophilic attacks.

4.11 Mulliken charges distribution

The well-known method for estimating atomic charges in the molecular orbital framework and for better understanding the electron distribution among atoms in a molecule is done by Mulliken population analysis [51, 52]. It plays a significant role in quantum chemistry calculations to molecular systems.

The charge displacement of the molecule is directly related to chemical bonds of the present compound. Therefore, it affects the dipole moment, polarizability, electronic structure and more properties of the molecular system. The net atomic charges of PTFA molecules obtained from Mulliken population analysis, are tabulated in Table 7. Figure 15 illustrates the atomic arrangement in PTFA compound demonstrates that the carbon atom attached with hydrogen atoms (C18, C12, C21, C9) is negative, whereas the remaining carbon atoms are positively charged due to these carbon atoms (C7, C6, C31, C32) attached with the high electro negative character of fluorine atom. In the same way, the positive charges are observed on the hydrogen atoms of the piperazine ring. It is worth mentioning that the highest values of charge are noticed for H16 & H25 likely due to hydrogen bonding interaction. The calculated results which exposed that the negative charge is delocalized across the nitrogen and oxygen atoms. Being with the intramolecular charge transfers also determined in the Mulliken charge analysis, the piperazine derivative occurs from the nitrogen and carbon atoms towards the oxygen atoms, which accept electron density that affects its electronic properties.

4.12 Nonlinear optical (NLO) study

The NLO properties of PTFA were investigated to understand its optoelectronic and photonic applications [53]. Theoretical studies of hyperpolarizabilities were conducted to evaluate its molecular nonlinear optical response. The calculations for the electronic dipole moment(μ), linear polarizability (α) and first-order hyper polarizability (β) of this compound have been calculated. The first-order hyperpolarizability, a third-rank tensor, is expressed as a $3 \times 3 \times 3$ matrix. Due to Kleinman symmetry [54], the 27 components of this matrix can be reduced to 10 independent components. The complete equation for calculating the magnitude of β_{tot} is given as follows:

$$\beta_{tot} = \left[(\beta_{xxx} + \beta_{xzz} + \beta_{xzz})^2 + (\beta_{yyy} + \beta_{yzz} + \beta_{xxy})^2 + (\beta_{zzz} + \beta_{xxz} + \beta_{yyz})^2 \right]^{1/2} \quad (1)$$

The calculated values of the total molecular dipole moment (μ_D), linear polarizability (α) and first-order hyperpolarizability (β_{tot}) have been obtained and are summarized in Table 8.

The values show that the dipole moment of the tested compound is $\mu_{tot} = 6.467$ D, with the largest contribution along the y-axis, where it measures 6.006 D, indicating a pronounced charge separation in this direction. Such a high dipole moment suggests efficient intramolecular charge transfer within the molecule. In addition, the computed total polarizability and first-order hyperpolarizability values are -145.111×10^{-24}e.s.u. and 170.319×10^{-31}e.s.u., respectively, indicating significant charge delocalization. Among the tensor components, the largest hyperpolarizability contributions arise mainly from the x-direction, particularly through β_{xyy}, β_{zxx}, and β_{zzz} components, which indicates that the electron cloud is more easily distorted along this axis. This maximum β value could result from π-electron cloud movement from donor to acceptor, which enhances molecular polarization and facilitates intramolecular charge transfer. The calculated total hyperpolarizability of PTFA (170.319×10^{-31} esu) is approximately 45.6 times that of urea, indicating an enhanced intrinsic molecular electronic polarization and charge-transfer response. These results reflect molecular-level optical response and do not imply macroscopic second-order nonlinear optical activity in the centrosymmetric crystal. These molecular properties may be relevant for understanding electronic and optical response in related systems.

5 Conclusion

In a novel approach, piperazine bis(trifluoroacetate) (PTFA) were studied using DFT/B3LYP/6–311 + + G (d, p) basis set method to determine the optimized geometrical parameters, electronic properties and its vibrational frequencies. The bond length and bond angles between the atoms are compared with the experimental results. In the crystal structure of PTFA was stabilized by the intermolecular interaction of N–H$\cdots$O. The Hirshfeld surface and 2D fingerprint plots show the intermolecular interactions of PTFA molecule.

In vibration, the N–H peak at 2854 cm^{-1} and theoretical peak at 2904 cm^{-1} are well correlated with the PED calculations. Using the same basis set, also calculated its electrical and optical properties of PTFA. The NBO analysis explains the inter and intra molecular interactions of PTFA molecules. It is possessed that

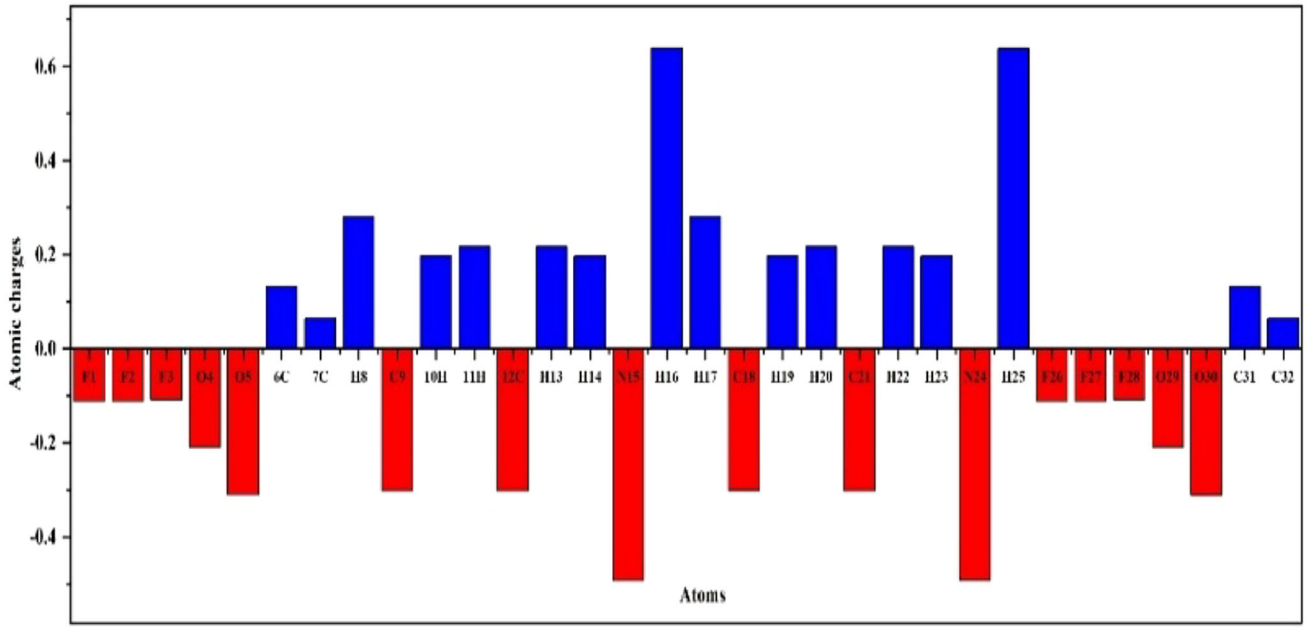

Fig. 15 Mulliken atomic charges of PTFA compound

Table 8 First order hyperpolarsability of PTFA compound

Parameters	B3LYP/6–311 + + G (d, p)	Parameters	B3LYP/6–311 + + G (d, p)
μ_x	0.678	β_{xxx}	− 17.829
μ_y	6.006	β_{xxy}	− 25.880
μ_z	2.301	β_{xyy}	70.173
μ(D)	6.467	β_{yyy}	− 58.369
α_{xx}	− 161.701	β_{zxx}	65.934
α_{xy}	6.700	β_{xyz}	6.711
α_{yy}	− 137.503	β_{zyy}	24.523
α_{xz}	− 11.714	β_{xzz}	22.577
α_{yz}	2.012	β_{yzz}	17.167
αzz	− 136.130	β_{zzz}	47.003
α_{tot} (e.s.u.) × 10^{-24}	− 145.111	β_{tot}(e.s.u.) × 10^{-31}	170.319

the strong stabilization, around 60 kcal/mol, arises from the lone pair electrons provided by the oxygen atoms. In the HOMO–LUMO analysis the energy gap (ΔE) is 6.591 eV, providing the minimum chemical reactivity and photochemical process with electron transfer. In the UV–Visible spectroscopy analysis the absorption spectrum for water, ethanol and methanol was identical, however, the absorption in the gas phase was higher. In addition, the reactive sites regions of the piperazine derivatives are found by MEP, ELF & LOL contour maps. Furthermore, the analysis of fukui and Mulliken charge atoms describes the differences in electro negativities and electro positivities of atoms within the molecule. The first order hyperpolarizability studies are also discussed to expose that PTFA compounds are suitable for NLO materials. Based on our findings, the chosen PTFA compound leads to better understanding and may contribute to favourable in more advanced applications in the field of photonics and material science.

Author contributions

V. Vijayalakshmi—Writing-original draft, Methodology, Conceptualization. K. Sivakumar—Formal analysis. V. Ragavendran—Data curation, Investigation. J. Janczak—Writing—review & editing, Visualization, Validation. N. Kanagathara*- Writing—review & editing, Validation, Methodology.

Data Availability Statement This manuscript has no associated data. [Author's comment: All data supporting this study will be provided based on request.]

Code Availability Statement This manuscript has no associated code/software. [Author's comment: Code/Software sharing not applicable to this article as no code/software was generated or analysed during the current study.]

Declarations

Conflicts of interest The authors have no conflict of interest to declare.

References

1. E. Jaziri, H. Louis, C. Gharbi, F. Lefebvre, W. Kaminsky, E.C. Agwamba, C. Egemonye, T.O. Unimuke, J. Ikenyirimba, G.E. Mathias, C.B. Nasr, L. Khedhiri, Investigation of crystal structures, spectral (FT-IR and NMR) analysis, DFT, and molecular docking studies of novel piperazine derivatives as antineurotic drugs. J. Mol. Struct. **1278**, 134937 (2023). https://doi.org/10.1016/j.molstruc.2023.134937
2. H. S. N. Prasad, A.P. Ananda, T.N. Lohith, P. Prabhuprasad, H.S. Jayanth, N.B. Krishnamurthy, M.A. Sridhar, L. Mallesha, P. Mallu, Design, synthesis, molecular docking and DFT computational insight on the structure of Piperazine sulfynol derivatives as a new antibacterial contender against superbugs MRSA, J. Mol. Struct., (1247) 2022, 131333. https://doi.org/10.1016/j.molstruc.2021.131333
3. K. Subashini, S. Periandy, Spectroscopic (FT-IR, FT-Raman, UV, NMR, NLO) investigation, molecular docking and molecular simulation dynamics on 1-Methyl-3-Phenylpiperazine, J. Mol. Struct., (1143) 2017, 328–343. https://doi.org/10.1016/j.molstruc.2017.04.016
4. S. Gunasekaran, B. Anita, Spectral investigation and normal coordinate analysis of piperazine. Appl. Phys. **46**, 833–838 (2008)
5. B. Praveena, D. Renuka Devee, R. Ranjani, N. Kanagathara, T. Sivanesan, Crystal growth, structural, spectral investigations, DFT calculations, thermal, photoluminescence, optical characteristics of a new organic material: piperidinium succinate (PS) single crystal, J Mater Sci: Mater Electron., 34 (581) 2023. https://doi.org/10.1007/s10854-023-09850-5
6. A. D. Steffy, D. Arul Dhas, I. Hubert Joe, B. Gunasekaran, G. Vinitha, Experimental and theoretical investigation on piperazine-1,4-diium bis (2,5-dichlorophenoxyacetate) single crystal: A potential candidate for nonlinear optical applications, J. M. Struct., 1285,2023,135520, 0022–2860. https://doi.org/10.1016/j.molstruc.2023.135520.
7. H.A. Ziyaei, E. Badali, DABCO bond cleavage for the synthesis of piperazine derivatives. RSC Adv. **9**, 36386–36409 (2019). https://doi.org/10.1039/C9RA07870C
8. E.A. Kallel, C. Vangel, D. Elbaum, Conformational analysis of 2- substituted piperazines. Bioorg. Med. Chem. Lett. **26–13**, 3010–3013 (2016). https://doi.org/10.1016/j.bmcl.2016.05.022
9. V. Sowmya, J. Lavanya, S. Yasodakrishna, B. Rajashaker, L. Nagarapu, B. Jagadeesh, B. Bala, J. Nishant, S. Sreekanth, M. Vijjulatha, A novel piperazine linked β-amino alcohols bearing a benzosuberone scaffolds as anti-proliferative agents, Bioorg. Med. Chem. Lett., 27 -4 (2017). https://doi.org/10.1016/j.bmcl.2017.01.031
10. A.W.M. Connaughie, J. Spychala, M. Zhao, D. Boykin, W.D. Wilson, Design and synthesis of RNA-specific groove-binding cations: implications for antiviral drug design. J. Med. Chem. **37**, 1063–1069 (1994). https://doi.org/10.1021/jm00034a004
11. D. Havlicek, J. Plocek, I. Nemec, R. Gyepes, Z. Micka, The crystal structure, vibrational spectra, and thermal behavior of piperazinium (2+) selenate monohydrate and N, N0 -Dimethylpiperazinium (2+) selenate dihydrate. J. Solid State Chem. **150–2**, 305–315 (2000). https://doi.org/10.1006/jssc.1999.8595
12. V. Krishnakumar, S. Seshadri, Scaled quantum chemical calculations and FT-IR, FT-Raman spectral analysis of 2-methyl piperazine, Spectrochim. Acta A Mol. Biomol. Spectrosc., 68–3 (2007), 833–838. https://doi.org/10.1016/j.saa.2006.12.067
13. A. Yokozeki, K. Kuchitsu, Molecular Structure of Piperazine as Studied by Gas Electron Diffraction. Bull. Chem. Soc. Jpn **44–9**, 2352–2355 (1971). https://doi.org/10.1246/bcsj.44.2352
14. L. W. Jenneskens, J. Mahy, E. M. M. de Brabander-van den Berg, I. van der Hoef, J. Lugtenburg, 2-(Trifluoromethyl)piperazine: Synthesis and characterization using NMR and X-ray photoelectron spectroscopy, Recl. Trav. Chim. Pays-Bas., 114–3 (1995), 97–102. https://doi.org/10.1002/recl.19951140305
15. G. Sudhakar, D. Rajan Babu, Growth and characterization of piperazine oxalic acid monochloride semiorganic NLO single crystals, Opt. Mater., 150 (2024), 115123. https://doi.org/10.1016/j.optmat.2024.115123
16. B. Raajaraman, N.R. Sheela, S. Muthu, Investigation on 1-Acetyl-4-(4-hydroxyphenyl) piperazine an anti-fungal drug by spectroscopic, quantum chemical computations and molecular docking studies. J. Mol. Struct. **1173**, 583–595 (2018). https://doi.org/10.1016/j.molstruc.2018.07.030
17. J. Priscilla, G. V. Vijayaraghavan, E. Paavai, M. Lakshmipriya, Crystal design of novel Piperazinum Isophthalate (PIP): growth, structural, thermal, spectral, mechanical and optical properties for NLO application, J. Mol. Struct., 1293 (2023),136307. https://doi.org/10.1016/j.molstruc.2023.136307
18. G. Parvathy, R. Kaliammal, K. Velsankar, G. Vinitha, K. Sankaranarayanan, R.M. Kumar, S. Sudhahar, Piperazinium bis (5-chlorosalicylate) - A new third order nonlinear optical single crystal, J. Mol. Struct., 1228 (2021),129728. https://doi.org/10.1016/j.molstruc.2020.129728
19. S. Arjunan, R.M. Kumar, R. Mohan, R. Jayavel, Growth and dielectric, mechanical, thermal and etching studies of an organic nonlinear optical L-arginine trifluoroacetate (LATF) single crystal. Mater. Res. Bull.

43(8–9), 2018–2025 (2008). https://doi.org/10.1016/j.materresbull.2007.10.008
20. V. Mathivanan, T. Raghavalu, M. Kovendhan, K. Suriya Kumar, S. Gokul Raj, G. Ramesh Kumar, R. Mohan, Synthesis and characterization of a new nonlinear optical single crystal: L-Lysinium trifluoroacetate, Cryst. Res. Technol., 43–3 (2008), 248–252. https://doi.org/10.1002/crat.200711056
21. B.S.I. Lasalle, M. Senthil Pandian, K. Anitha, P. Ramasamy, Growth of piperazinium bis (trifluoroacetate)(PTFA) single crystal for nonlinear optical (NLO) application, J. Mater. Sci.: Mater. Electron., 34 (2023), 1527. https://doi.org/10.1007/s10854-023-10945-2
22. M. Frisch, F. Clemente, MJ Frisch, GW Trucks, HB Schlegel, GE Scuseria, MA Robb, JR Cheeseman, G. Scalmani, V. Barone, B. Mennucci, GA Petersson, H. Nakatsuji, M. Caricato, X. Li, HP Hratchian, AF Izmaylov, J. Bloino. G. Zhe, Gaussian16.
23. M.H. Jamroz, Vibrational energy distribution analysis (VEDA): scopes and limitations, Spectrochim. Acta Part A Mol. Biomol. Spectrosc. **114**, 220–230 (2013). https://doi.org/10.1016/j.saa.2013.05.096
24. G.A. Zhurko, D. A. Zhurko, Chemcraft Program Version 1.6(Build 315). 2009.
25. R.D. Dennington, T.A. Keith, J.M. Millam, GaussView 5.0.8, Inc., 2008
26. T. Lu, F. Chen, Multiwfn: a multifunctional wavefunction analyzer. J. Comput. Chem. **33–5**, 580–592 (2012). https://doi.org/10.1002/jcc.22885
27. M. J. Turner, J. J. McKinnon, S. K. Wolff, D. J. Grimwood, P. R. Spackman, D. Jayatilaka and M. A. Spackman, CrystalExplorer17 (2017). University of Western Australia.
28. C. Karnan, A. Ramkumar, S. Selvaraj, Quantum Chemical Computational Studies on the Structural Aspects, Spectroscopic Properties, Hirshfeld Surfaces, Donor-Acceptor Interactions and Molecular Docking of Clascosterone: A Promising Antitumor Agent, Int. Res. J. Multidiscip. Technovation., (2024). https://doi.org/10.54392/irjmt2444
29. C. Karnan, K. Nagaraja, S. Manivannan, Crystal structure, spectral investigations, DFT and antimicrobial activity of brucinium benzilate (BBA). J. Mol. Model. **27**, 223 (2021). https://doi.org/10.1007/s00894-021-04842-w
30. K.W. Wang, Z.M. Jin, Y. JiangPan, Crystal structure of the piperazine-1,4-diium (DL-)hydrogen malate (1:2). J. Chem. Crystallogr. **35**, 413–417 (2005). https://doi.org/10.1007/s10870-005-2213-9
31. J.S. Kumar, T.S.R. Devi, G.R. Ramkumaar, A. Bright, Ab initio and density functional theory calculations of molecular structure and vibrational spectra of 4-(2-Hydroxyethyl) piperazine-1-ethanesulfonic acid, Spectrochim. Acta Part A Mol. Biomol. Spectrosc. **152**, 509–522 (2015). https://doi.org/10.1016/j.saa.2015.07.084
32. O. Alver, C. Parlak, M. Senyel, FT-IR and NMR investigation of 1- phenylpiperazine: a combined experimental and theoretical study, Spectrochim. Acta Part A Mol. Biomol. Spectrosc. **67**(3–4), 793–801 (2007). https://doi.org/10.1016/j.saa.2006.08.035
33. N. Prabavathi, A. Nilufer, V. Krishnakumar, FT-IR, FT-Raman and DFT quantum chemical study on the molecular conformation, vibrational and electronic transitions of 1-(m-(trifluoromethyl)phenyl) piperazine, Spectrochim. Acta Part A Mol. Biomol. Spectrosc. **121**, 483–493 (2014). https://doi.org/10.1016/j.saa.2013.10.102
34. V. Sangeetha, M. Govindarajan, N. Kanagathara, M.K. Marchewka, S. Gunasekaran, G. Anbalagan, Structure and vibrational spectra of melaminium bis(trifluoroacetate) trihydrate: FT-IR, FT-Raman and quantum chemical calculations, Spectrochim. Acta Part A Mol. Biomol. Spectrosc., (125) 2014, 252–263. https://doi.org/10.1016/j.saa.2014.01.018
35. L.J. Bellamy, The Infrared Spectra of Complex Molecules, Chapman and Hall/ Wiley, London/New York, 1975.
36. S. Sevvanthi, S. Muthu, M. Raja, S. Aayisha, S. Janani, PES, molecular structure, spectroscopic (FT-IR, FT-Raman), electronic (UV-Vis, HOMO-LUMO), quantum chemical and biological (docking) studies on a potent membrane permeable inhibitor: dibenzoxepine derivative, Heliyon, 6 -8 (2020). https://doi.org/10.1016/j.heliyon.2020.e04724
37. M. Govindarajan, M. Karabacak, Spectroscopic properties, NLO, HOMO–LUMO and NBO analysis of 2,5-Lutidine, Spectrochim. Acta Part A Mol. Biomol. Spectrosc. **96**, 421–435 (2012). https://doi.org/10.1016/j.saa.2012.05.067
38. N. Kanagathara, F. MaryAnjalin, V. Ragavendran, D. Dhanasekaran, R. Usha, R. Rao, M.K. Marchewka, Experimental and Theoretical (DFT) investigation of Crystallographic, Spectroscopic and Hirshfeld surface analysis of anilinium arsenate. J. Mol. Struct. **1223**, 128965 (2020). https://doi.org/10.1016/j.molstruc.2020.12896
39. O. Noureddine, S. Gatfaoui, S.A. Brandán, H. Marouani, N. Issaoui, Structural, docking and spectroscopic studies of a new piperazine derivative, 1-phenylpiperazine-1,4-diium-bis (hydrogen sulfate), J. Mol. Struct., 127351. https://doi.org/10.1016/j.molstruc.2019.127351
40. P. Rajkumar, S. Selvaraj, P. Anthoniammal, A. Ram Kumar, K. Kasturi, S. Kumaresan Structural (monomer and dimer), spectroscopic (FT-IR, FT-Raman, UV–Vis and NMR) and solvent effect (polar and nonpolar) studies of 2-methoxy-4-vinyl phenol, Chem. Phys. Impact.,7 (2023),100257. https://doi.org/10.1016/j.chphi.2023.100257
41. N. Prabavathi, N. Senthil Nayaki, V. Krishnakumar, Spectroscopic investigation (FT-IR, FT-Raman, NMR and UV-Vis), conformational stability, NBO and thermodynamic analysis of 1-(2-methoxyphenyl) piperazine and 1-(2-chlorophenyl) piperazine by DFT approach, Pharm. Anal. Acta, 2–6 (2015). https://doi.org/10.4172/2153-2435.1000391
42. A. Bendjeddou1, T. Abbaz1, A. K. Gouasmia, D. Villemin, Molecular Structure, HOMO-LUMO, MEP and Fukui Function Analysis of Some TTF-donor Substituted Molecules Using DFT (B3LYP) Calculations, Int. Res. J. Pure Appl. Chem., (2016), 1–9. https://doi.org/10.9734/IRJPAC/2016/27066
43. B. wang, C. Rong, K. Pratim, C. Shubin Liu, comparative study to predict regioselectivity, electrophilicity and nucleophilicity with Fukui function and Hirshfeld

charge, Theor Chem Acc., 138–124 (2019). https://doi.org/10.1007/s00214-019-2515-1
44. K. Arulaabaranam, S. Muthu, G. Mani, A.S. Ben Geoffrey, Speculative assessment, molecular composition, PDOS, topology exploration (ELF, LOL, RDG), ligand-protein interactions, on 5-bromo-3-nitropyridine-2-carbonitrile, Heliyon, 7–5 (2021). https://doi.org/10.1016/j.heliyon.2021.e07061
45. M. Sumithra, N. Sundaraganesan, R. Rajesh, V. Vetrivelan, V. Ilangovan, S. Javed, S. Muthu, Electron acceptor, excitation energies, oscillatory strength, spectroscopic and solvent effects on 5-amino-4,6-dichloro-2-(propylthio) pyrimidine - anticancer agent. Chem. Phys. Impact. **6**, 1000145 (2023). https://doi.org/10.1016/j.chphi.2022.100145
46. F. Basha, F. L. Ali Khan, S. Muthu, M. Raja, Computational evaluation on molecular structure (Monomer, Dimer), RDG, ELF, electronic (HOMO-LUMO, MEP) properties, and spectroscopic profiling of 8-Quinolinesulfonamide with molecular docking studies, Comput. Theor. Chem., 1198 (2021), 113169. https://doi.org/10.1016/j.comptc.2021.113169.
47. N. Shanmugapriya, V. Balachandran, B. Revathi, B. Narayana, Vinutha V. Salian, K. Vanasundari, C. Sivakumar, Quantum chemical calculation, performance of selective antimicrobial activity using molecular docking analysis, RDG and experimental (FT-IR, FT-Raman) investigation of 4-[{2-[3-(4-chlorophenyl)-5-(4-propan-2-yl) phenyl)-4, 5-dihydro- 1H- pyrazol-1-yl]-4-oxo-1, 3- thiazol-5(4H)-ylidene} methyl] benzonitrile, Heliyon, 7 -7 (2021). https://doi.org/10.1016/j.heliyon.2021.e07634
48. K. Arulaabaranam, S. Muthu, G. Mani, A.S. Ben Geoffrey, speculative assessment, molecular composition, PDOS, topology exploration (ELF, LOL, RDG), ligand-protein interactions, on 5-bromo-3-nitropyridine-2-carbonitrile, Heliyon, 7–5(2021). https://doi.org/10.1016/j.heliyon.2021.e07061
49. S. Muthu, S. Renuga, Vibrational spectra and normal coordinate analysis of 2-hydroxy-3-(2-methoxyphenoxy) propyl carbamate. Spectroc. Acta Pt. A-Molec. Biomolec. **132**, 313–325 (2014). https://doi.org/10.1016/j.saa.2014.05.009
50. N. Prabavathi, N. Senthil Nayaki, V. Krishnakumar, Spectroscopic Investigation (FT-IR, FT-Raman, NMR and UV-Vis), Conformational Stability, NBO and Thermodynamic Analysis of 1-(2-Methoxyphenyl) Piperazine and 1-(2-Chlorophenyl) Piperazine by DFT Approach, Pharm Anal Acta.,(2015). https://doi.org/10.4172/2153-2435.1000391
51. S. Selvaraj, P. Rajkumar, M. Kesavan, S. Gunasekaran, S. Kumaresan, Experimental and theoretical investigations on spectroscopic properties of tropicamide, J. Mol. Struct., 1173 (2018), 52–62. https://doi.org/10.1016/j.molstruc.2018.06.097
52. S. Azhagiri, S. Jayakumar, S. Gunasekaran, S. Srinivasan, Molecular structure, Mulliken charge, frontier molecular orbital and first hyperpolarizability analysis on 2-nitroaniline and 4-methoxy-2-nitroaniline using density functional theory. Spectroc. Acta Pt. A-Molec. Biomolec. **124**, 199–202 (2013). https://doi.org/10.1016/j.saa.2013.12.106
53. P. Jayaprakash, R. Ramachandran, S. Selvaraj, Quantum computational investigation into the optoelectronic and NLO properties of C8H8O3. C3H7NO2 single crystal, J. Mol. Struct., 1319 (2025): 139488. https://doi.org/10.1016/j.molstruc.2024.139488
54. S. Muthu, G. Ramachandran, Spectroscopic studies (FTIR, FT-Raman and UV–Visible), normal coordinate analysis, NBO analysis, first order hyper polarizability, HOMO and LUMO analysis of (1R)-N-(Prop-2-yn-1-yl)-2,3-dihydro-1H-inden-1-amine molecule by ab initio HF and density functional methods. Spectrochim Acta A Mol Biomol Spectrosc. **121**, 394–403 (2014). https://doi.org/10.1016/j.saa.2013.10.093